A One Dimensional Model for the Dynamics of Confined Granular Avalanches

Stefano De Toni[1)] and Paolo Scotton[2)]
1) PhD, Department of Civil and Environmental Engineering, University of Trento, Via Mesiano 77, 38050 Trento, Italy (stefano.detoni@ing.unitn.it)
2) Assistant professor, Department of Civil and Environmental Engineering, University of Trento, Via Mesiano 77, 38050 Trento, Italy (paolo.scotton@ing.unitn.it)

Abstract

The zoning of avalanche hazard is one of the main tasks of land-use planning in alpine areas. In Italy avalanche registers collect records of avalanche events only since a limited period of time and the low frequency of occurrence of snow avalanches in some sites makes it difficult to perform a statistical analysis of these data. Old documents, interviews with the inhabitants and field analysis (dendrochronological analysis for instance) supply further informations, useful for avalanche risk area mapping. Simulations made with physical and mathematical model can improve the knowledge of the dynamics of these events. A one dimensional model for confined granular avalanches, written in a curvilinear coordinate system, has been developed. Given the topography, the initial volume, the parameters which represents the resistance due to the interaction with the bottom and the sides of the channel, the model returns the evolution of profiles of running depth and velocity and the configuration of final deposit. Most of snow avalanches which take place in alpine regions in Italy are granular avalanches and this justifies the choice of the rheology proposed by Savage and Hutter for granular flows. The medium is treated as an incompressible continuum, characterized by a Mohr-Coulomb type yield criterion, parametrized through ϕ, the internal friction angle. The interaction of the moving mass with the soil is represented through a Coulomb-type frictional law, based on the parameter δ_b, the bottom friction angle. New rheological hypotheses have been introduced in order to describe, through a lateral friction angle δ_{lat}, the frictional interaction with vertical sides. The model has been tested against experimental data relevant to cases with constant width, obtained from an experimental campaign carried out at the Hydraulic Laboratory of the University of Trento.

Keywords: snow avalanche, granular rheology, hazard zoning

Introduction

In the Province of Trento, in Italy, new regulations for hydrological risk zoning are being developed, in order to differentiate the use of the territory depending on the hazard level. In the case of snow avalanches different tools can help collecting informations useful to draw the map of risk: historical archives, interviews, field analysis (like dendrochronological studies), photo-interpretation. Numerical models can improve the knowledge of the catastrophic events that can affect an area, helping in the discrimination of various degrees of intensity of the events. Given the topography of the terrain, the position, the distribution and the volume of the initial mass, a representation of the interaction of the medium with the boundary, the model returns the evolution of some dynamic parameters (depth, velocity) during the motion of the mass. A good quality of mathematical models is that the parameters, introduced to describe the behaviour of the material, preserve their physical meaning, in order to confine the uncertainty of the simulation to the definition of the initial and boundary conditions.

In the field of snow dense avalanches and dry granular fluxes, numerical models based on the theory by Hutter and Savage (Savage and Hutter (1989), Savage and Hutter (1991)) are demonstrating their reliability, in laboratory experiments (De Toni et al. (2004), De Toni (2005), De Toni and Scotton (2005)) and in the application to real cases (Scotton (1999), Barberi and Scotton (2004)). In the theory of Hutter and Savage the medium, a dry granular material, can be treated as a continuum, because of the small size of particles compared to the characteristic sizes of the moving mass. This hypothesis is surely acceptable for most of dense granular gully avalanches, object of this study, since the characteristic size of snow particle ranges between $1\,cm$ and $50\,cm$, usually much smaller than the flowing depth. The authors registered flowing depths of 8–$10\,m$ relevant to channel avalanches occurred in various sites in the north of Italy, near to Trento (e.g. Val dei Spini (Scotton (1999)) and Lavina Granda (De Toni (2005))). The material is assumed to be incompressible; only in the very initial stages of the motion a strong dilatation of the granular material occurs, without affecting the following

pp. 275–287

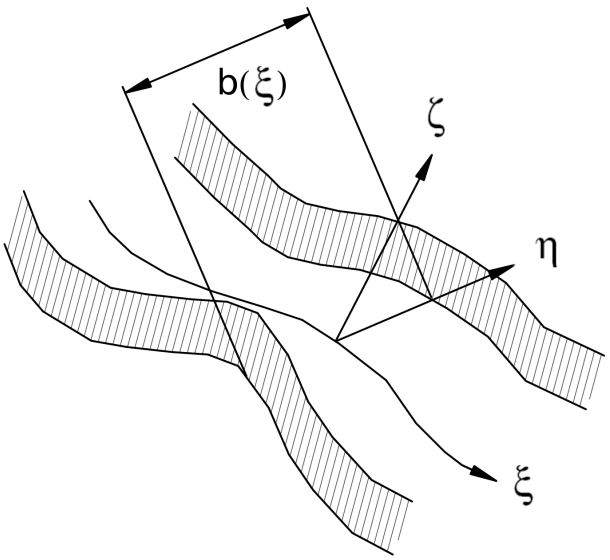

Fig. 1. The curvilinear coordinate system (ξ, η, ζ).

dynamic. The "shallow water" hypothesis is applied, since the flowing depth is usually small compared to the longitudinal dimensions of the mass. A Mohr-Coulomb type yield criterion, parametrized through the internal friction angle ϕ, is applied to describe the failure conditions. The granular mass is assumed to slide over the bottom as in a "plug flow"; the interaction with the sliding surface is described through a Coulomb type frictional law, with a bottom friction angle δ_b, smaller than ϕ.

Recently Pudasaini et alii have developed a two dimensional depth integrated model for granular flows over gently curved and twisted topographies (Pudasaini and Hutter (2003), Pudasaini et al. (2004), Pudasaini et al. (2005)). That model can investigate cases with moderate lateral confinement. In avalanches occurring in topographies with strong lateral confinement (couloir avalanches), it is conceivable that the lateral friction plays an important role. A research is in progress at the Department of Civil and Environmental Engineering of the University of Trento in order to study the effects of lateral walls in rectangular sections, to develop a one dimensional model with variable width. In this article the field of discussion is restricted to the case with constant width, aiming to focus on various rheological choices applicable to describe the stresses which arise at the lateral sides.

The mathematical model.

The equations of motion are developed in a three dimensional curvilinear coordinate system, shown in Fig. 1, where ζ is normal to the bottom, ξ runs along the channel and η is normal to ξ and ζ.

The continuity equation in scalar form is:

$$\frac{1}{1-\chi\zeta}\,\frac{\partial u_\xi}{\partial \xi} + \frac{\partial u_\eta}{\partial \eta} + \frac{\partial u_\zeta}{\partial \zeta} - \frac{\chi}{1-\chi\zeta}\,u_\zeta = 0\,, \tag{1}$$

where u_i is the component of the velocity vector in the generic direction i and χ is the curvature. The

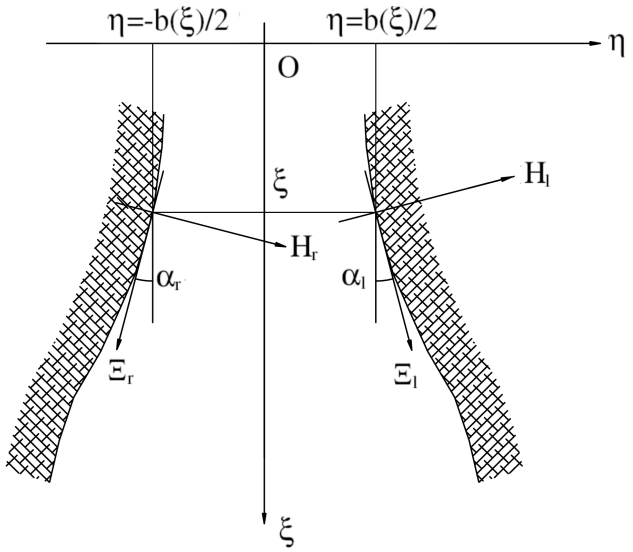

Fig. 2. The auxiliary (Ξ, H)-local coordinate systems relevant to the left and right banks.

momentum balance equations in the three directions ξ, η and ζ are:

$$\begin{aligned}\frac{\partial u_\xi}{\partial t} &+ \frac{u_\xi}{1-\chi\zeta}\frac{\partial u_\xi}{\partial \xi} + u_\eta \frac{\partial u_\xi}{\partial \eta} + u_\zeta \frac{\partial u_\xi}{\partial \zeta} - \frac{\chi}{1-\chi\zeta} u_\xi u_\zeta = \\ &= g\,\sin\beta + \frac{1}{\rho}\left(\frac{1}{1-\chi\,\zeta}\frac{\partial p_{\xi\xi}}{\partial \xi} + \frac{\partial p_{\eta\xi}}{\partial \eta} + \frac{\partial p_{\zeta\xi}}{\partial \zeta} - \frac{2\,\chi}{1-\chi\zeta}\,p_{\zeta\xi}\right), \end{aligned} \tag{2}$$

$$\begin{aligned}\frac{\partial u_\eta}{\partial t} &+ \frac{u_\xi}{1-\chi\zeta}\frac{\partial u_\eta}{\partial \xi} + u_\eta \frac{\partial u_\eta}{\partial \eta} + u_\zeta \frac{\partial u_\eta}{\partial \zeta} = \\ &= \frac{1}{\rho}\left(\frac{1}{1-\chi\,\zeta}\frac{\partial p_{\xi\eta}}{\partial \xi} + \frac{\partial p_{\eta\eta}}{\partial \eta} + \frac{\partial p_{\zeta\eta}}{\partial \zeta} - \frac{\chi}{1-\chi\zeta}\,p_{\zeta\eta}\right), \end{aligned} \tag{3}$$

$$\begin{aligned}\frac{\partial u_\zeta}{\partial t} &+ \frac{u_\xi}{1-\chi\zeta}\frac{\partial u_\zeta}{\partial \xi} + u_\eta \frac{\partial u_\zeta}{\partial \eta} + u_\zeta \frac{\partial u_\zeta}{\partial \zeta} + \frac{\chi}{1-\chi\zeta} u_\xi^2 = \\ &= -g\,\cos\beta + \frac{1}{\rho}\left(\frac{1}{1-\chi\,\zeta}\frac{\partial p_{\xi\zeta}}{\partial_l \xi} + \frac{\partial p_{\eta\zeta}}{\partial \eta} + \frac{\partial p_{\zeta\zeta}}{\partial \zeta} - \frac{\chi}{1-\chi\zeta}\,(p_{\xi\xi} - p_{\zeta\zeta})\right), \end{aligned} \tag{4}$$

being p_{ij} the component in the direction j of the stress vector acting on a plane normal to i. Traction normal stress are assumed positive. β is the local slope angle. Being H_s, B_s and L_s the depth, transversal and longitudinal length scales and R_s the scale of the radius of curvature of bed profile, it is assumed that $\lambda = L_s/R_s \approx 1$ and $\varepsilon = H_s/L_s \lll 1$ ("shallow water" hypothesis). Non-dimensionalizing the momentum balance equations and assuming that inertial, gravitational and pressure forces are comparable, neglecting the lower order terms, the equations of motion in the directions η (3) and ζ (4) become:

$$\frac{\partial p_{\eta\eta}}{\partial \eta} + \frac{\partial p_{\zeta\eta}}{\partial \zeta} = 0\,. \tag{5}$$

$$\frac{\partial p_{\zeta\zeta}}{\partial \zeta} + \frac{\partial p_{\eta\zeta}}{\partial \eta} = \rho\left(g\,\cos\beta + \chi\,u_\xi^2\right), \tag{6}$$

The components of the stress tensor are initially defined at the left and right bottom corners of the rectangular section, on local auxiliary coordinate systems $(\Xi, H)_{l/r}$ relevant to the orientation of the left (l) and right (r) lateral banks (see Fig. 2):

$$\left(\tilde{\mathbf{P}}\right)_{l/r} = \begin{pmatrix} p_{\Xi\Xi} & (p_{\Xi H})_{l/r} & p_{\Xi\zeta} \\ (p_{H\Xi})_{l/r} & (p_{HH})_{l/r} & p_{\Xi\zeta} \\ p_{\zeta\Xi} & p_{\zeta H} & p_{\zeta\zeta} \end{pmatrix}.$$

The dynamic boundary conditions at the bottom and at the lateral walls are described through a Coulomb type friction law. Given that there is no component of velocity transversal to Ξ, due to the kinematic boundary

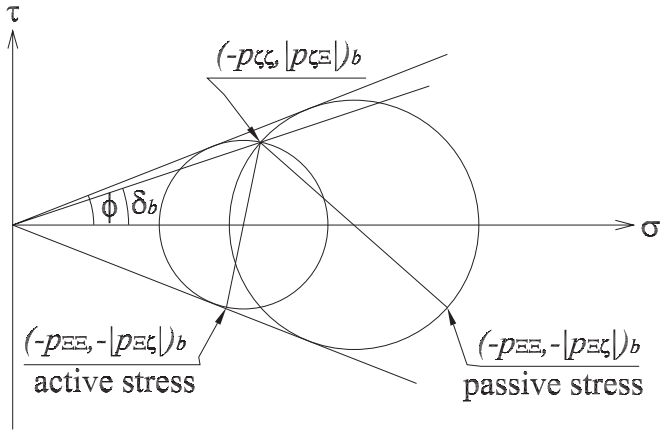

Fig. 3. The definition of the stress tensor components on the plane $\Xi\zeta$, according to the Savage-Hutter theory (1989).

condition, the tangential stress oriented along the curvilinear coordinate ξ are, at the bottom, left and right sides:

$$\begin{aligned} p_{\zeta\Xi} &= +sgn\,(u_\xi)\,\tan\delta_b\,p_{\zeta\zeta}\,, \\ (p_{H\Xi})_l &= +sgn\,(u_\xi)\,\tan\delta_{lat}\,(p_{HH})_l\,, \\ (p_{H\Xi})_r &= -sgn\,(u_\xi)\,\tan\delta_{lat}\,(p_{HH})_r\,. \end{aligned}$$

Assuming secondary circulations and stresses of smaller magnitude, we can consider $p_{\Xi H} = p_{H\Xi} \approx 0$.

The Mohr-Coulomb type yield criterion, applied to the coordinate plane $\Xi\zeta$, allows to evaluate $p_{\Xi\Xi}$'s dependence on $p_{\zeta\zeta}$. On the Mohr diagram, the circle which defines the stress state on the plane $\Xi\zeta$ must pass through the point $(-p_{\zeta\zeta}, |p_{\zeta\Xi}|)$ and has to be tangential to the yield envelope with slope ϕ (see Fig. 3). Two circles respect the imposed conditions. The one which corresponds to a greater value of $-p_{\Xi\Xi}$ is associated to the passive state, which, in the theory of Hutter and Savage, takes place when $\partial u_\xi/\partial\xi < 0$. The other circle represents the active stress state, occurring when $\partial u_\xi/\partial\xi > 0$. It results that:

$$p_{\Xi\Xi} = \kappa^\zeta_{a/p}\,p_{\zeta\zeta}\,,$$

where $k^\zeta_{a/p}$, depending on the sign of $\partial u_\xi/\partial\xi$, is equal to k^ζ_a or k^ζ_p, defined as:

$$\left\{ \begin{matrix} k^\zeta_p \\ k^\zeta_a \end{matrix} \right\} = \frac{2}{cos^2\phi}\left[1 \pm \sqrt{1 - \frac{cos^2\phi}{cos^2\delta_b}}\right] - 1\,, \quad \text{if} \quad \frac{\partial u_\xi}{\partial\xi} \lessgtr 0\,.$$

The main task in the definition of the component of the three dimensional stress tensor is the representation of the transversal pressure p_{HH}. Hutter et al. (1993), developed a two dimensional model for the motion of a granular mass down an inclined plane, assuming that the transversal direction is principal. Tangential lateral stress is small compared to the longitudinal pressure and to the tangential stress at the bottom. The same hypothesis is assumed to be valid by Pudasaini and Hutter (2003) for granular avalanches moving down curved and twisted channels, with slightly varying topographies. If the granular motion occurs in a confined channel, lateral friction stresses are no more negligible and so the transversal pressure p_{HH} cannot be considered principal. Four different alternatives for the representation of p_{HH} are going to be analysed in this article.

- The simplest choice is to consider p_{HH} always equal to $p_{\zeta\zeta}$:

$$p_{HH} = k_{HH}\,p_{\zeta\zeta} = 1 \cdot p_{\zeta\zeta} \quad \Rightarrow \quad k_{HH} = 1\,. \tag{7}$$

  In this way, possible variations of the transversal pressure, due to relaxation or thickening movements of the mass, are not taken into account. The transversal pressure is assumed hydrostatic.

A different approach is to characterize the stress state on the plane ΞH, applying the procedure introduced by Hutter and Savage. Two circles, tangential to the material yield locus defined by the internal friction angle ϕ,

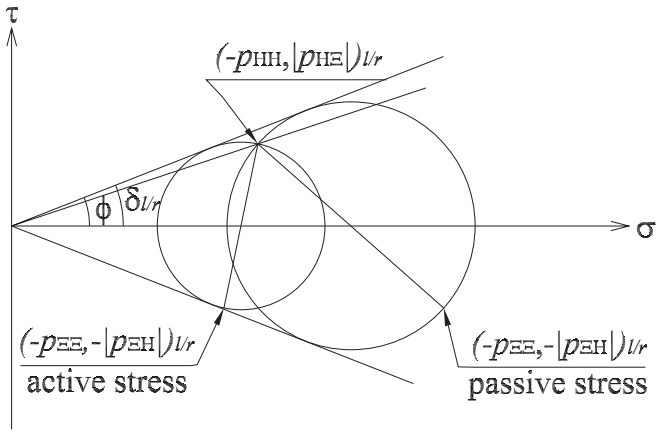

Fig. 4. The definition of the stress tensor components on the plane ΞH.

can be drawn through the point $(-p_{HH}, |p_{H\Xi}|)$ (see Fig. 4). It results:

$$\kappa^H_{a/p} p_{\Xi\Xi} = \kappa^H_{a/p}\, p_{HH} \quad \Rightarrow \quad p_{HH} = \frac{p_{\Xi\Xi}}{\kappa^H_{a/p}} = \frac{\kappa^\zeta_{a/p}}{\kappa^H_{a/p}}\, p_{\zeta\zeta} = k_{HH}\, p_{\zeta\zeta}\,,$$

where $k^H_{a/p}$ can be equal to k^H_a or k^H_p, defined as:

$$\left\{ \begin{array}{c} k^H_p \\ k^H_a \end{array} \right\} = \frac{2}{cos^2\phi} \left[1 \pm \sqrt{1 - \frac{cos^2\phi}{cos^2\delta_{lat}}} \right] - 1\,.$$

Different criteria can be applied to distinguish between active and passive state. We consider three cases. The former two represent the extreme conditions according to this approach.

- the transversal stress coefficient $\kappa^H_{a/p}$ is considered always equal to the active one, that is $p_{\Xi\Xi}$ is active with respect to the transversal pressure p_{HH} and so p_{HH} is always greater than $p_{\Xi\Xi}$:

$$p_{HH} = \frac{\kappa^\zeta_{a/p}}{k^H_a}\, p_{\zeta\zeta} \quad \Rightarrow \quad k_{HH} = \frac{\kappa^\zeta_{a/p}}{k^H_a}\,; \tag{8}$$

- $\kappa^H_{a/p}$ is always equal to the passive one, i.e. $p_{\Xi\Xi}$ is passive with respect to the transversal pressure p_{HH} and so p_{HH} is always smaller than $p_{\Xi\Xi}$:

$$p_{HH} = \frac{\kappa^\zeta_{a/p}}{k^H_p}\, p_{\zeta\zeta} \quad \Rightarrow \quad k_{HH} = \frac{\kappa^\zeta_{a/p}}{k^H_p}\,; \tag{9}$$

- the transversal stress coefficient $\kappa^H_{a/p}$ is equal either to the passive one or to 1, depending on the relaxing or thickening conditions of the moving mass. If the mass is elongating the transversal pressure is assumed equal to the longitudinal active one. If the mass is contracting, the longitudinal pressure is assumed passive with respect to the transversal one, that is it is assumed that the longitudinal thickening does not result in a transversal compression:

$$p_{HH} = \frac{k^\zeta_a}{1}\, p_{\zeta\zeta} \quad \Rightarrow \quad k_{HH} = k^\zeta_a\,, \quad \text{if} \quad \frac{\partial u_\xi}{\partial \xi} > 0\,, \tag{10}$$

$$p_{HH} = \frac{k^\zeta_p}{k^H_p}\, p_{\zeta\zeta} \quad \Rightarrow \quad k_{HH} = \frac{k^\zeta_p}{k^H_p}\,, \quad \text{if} \quad \frac{\partial u_\xi}{\partial \xi} < 0\,. \tag{11}$$

For all these cases, the stress tensor at the bottom corners of the rectangular section depends linearly on $p_{\zeta\zeta}$:

$$\begin{aligned} \left(\tilde{\mathbf{P}}\right)_{l/r} &= \begin{pmatrix} \kappa^\zeta_{a/p} & \pm sgn\,(u_\xi)\; k_{HH}\; \tan\delta_{lat} & -sgn\,(u_\xi)\; \tan\delta_b \\ \pm sgn\,(u_\xi)\; k_{HH}\; \tan\delta_{lat} & k_{HH} & 0 \\ -sgn\,(u_\xi)\; \tan\delta_b & 0 & 1 \end{pmatrix} p_{\zeta\zeta} = \\ &= \left(\tilde{\mathbf{K}}\right)_{l/r}\, p_{\zeta\zeta}\,. \end{aligned}$$

It is assumed that this linear dependence is valid across the entire section.

The components of the stress tensor $(\mathbf{P})_{l/r}$ in the (ξ,η,ζ)-coordinate system are obtained rotating $\left(\tilde{\mathbf{P}}\right)_{l/r}$ by the angle $(\alpha)_{l/r}$ between $(\Xi)_{l/r}$ and ξ (see Fig. 2):

$$(\mathbf{P})_{l/r} = \left(\mathbf{R}\,\tilde{\mathbf{P}}\,\mathbf{R}^T\right)_{l/r} = \left(\mathbf{R}\,\tilde{\mathbf{K}}\,\mathbf{R}^T\right)_{l/r} p_{\zeta\zeta} = (\mathbf{K})\; p_{\zeta\zeta}\,,$$

where $(\mathbf{R})_{l/r}$ is the rotation matrix associated to $(\alpha)_{l/r}$. Integrating the ζ motion equation (6) over η in the range between $-b/2$ and $b/2$ (where b is the width) and over ζ in the range between ζ and h (being h the flowing depth), assuming $p_{\zeta\eta} = p_{\eta\zeta} = 0$ and u_ξ and h constant over the entire section, imposing a null stress dynamic boundary condition at the free surface, one obtains the hydrostatic pressure distribution:

$$\hat{p_{\zeta\zeta}} = -\rho\left(g\,\cos\beta + \chi\,u_\xi^2\right)\left(h\,(\xi,t) - \zeta\right)\,, \quad \text{being} \quad \hat{p_{\zeta\zeta}} = \frac{1}{b}\int_{-b/2}^{b/2} p_{\zeta\zeta}\,d\eta\,.$$

equation (5), in the hypothesis that $p_{\zeta\eta} = p_{\eta\zeta} = 0$, tells that $p_{\eta\eta}$ must be constant over h. This suggests to consider a linear distribution of the stress tensor coefficients over η across the section:

$$\begin{aligned}\mathbf{P}\,(\xi,\,\eta,\,\zeta,\,t) &= -\mathbf{K}\,(\xi,\,\eta,\,t)\;\hat{p_{\zeta\zeta}}\;(\xi,\,\zeta,\,t) = \\ &= -\frac{\mathbf{K}_l\,(\xi,\,t)\cdot(b/2+\eta) + \mathbf{K}_r\,(\xi,\,t)\cdot(b/2-\eta)}{b}\cdot \\ &\quad\cdot\rho\left(g\,\cos\beta\,(\xi) + \chi\,(\xi)\;u_\xi^2\,(\xi,\,t)\right)\left(h\,(\xi,t) - \zeta\right)\,.\end{aligned}$$

Under this hypothesis it is possible to integrate the continuity equation (1) and the momentum balance equation along ξ (2) over the entire section:

$$\frac{\partial h}{\partial t} + \frac{\partial\,(h\,U_\xi)}{\partial\xi} = 0 \tag{12}$$

$$\frac{\partial U_\xi}{\partial t} + U_\xi\,\frac{\partial U_\xi}{\partial\xi} - \chi\,U_\xi\,U_\zeta = g\,\sin\beta + \frac{1}{b\,h}\left[b\,\frac{\partial\,(h\,P_{\xi\xi})}{\partial\xi} + h\left((P_{\eta\xi})_l - (P_{\eta\xi})_r\right) - 2\,b\,P_{\zeta\xi}\right] \tag{13}$$

$$\text{being} \quad U_i = \frac{1}{b}\int_{-b/2}^{b/2}\left(\int_0^h u_i\,d\zeta\right)d\eta \quad \text{and} \quad P_{ij} = \frac{1}{b}\int_{-b/2}^{b/2}\left(\int_0^h P_{ij}\,d\zeta\right)d\eta$$

The numerical model.

The averaged motion equations are solved by means of a lagrangian finite difference method, thoroughly described in De Toni (2005). Four different versions of the model have been developed corresponding to the four alternative definitions of the transversal pressure $p_{\eta\eta}$: $v1.3.3.1$ corresponds to equation (8); $v1.4.3.1$ corresponds to equation (7); $v1.5.3.1$ corresponds to equation (9); $v1.6.3.1$ corresponds to equations (10) and (11).

The laboratory experiments.

At the Hydraulic Laboratory of the University of Trento a campaign of experiments has been carried out in order to test the one dimensional model for confined granular avalanches. The experimental apparatus consists of a channel, with rectangular section, mounted on two inclined planes, with adjustable slope, connected with a narrow flexible strip (see Fig. 5). The planes are in forex, the transparent lateral sides of the rectangular channel in perspex. A granular mass is released from rest conditions, by manually lifting a sliding gate, inclined of 68^o on the upper plane. The granular material is represented by synthetic zeolite, an anionic resin, having dimensions which range from $0.1\,mm$ to $2\,mm$, but with a low dispersion around the mean diameter of $1\,mm$. The static values of the internal, bottom and lateral friction angles, have been measured by means of a shear box (De Toni (2005)) ($\phi = 28^o \pm 0.75^o$; $\delta_{lat} = 18^o \pm 0.75^o$; $\delta_b = 22^o \pm 0.75^o$). The evolution of the motion has been shot laterally and from above by means of three video-cameras (see Fig. 6): a Canon Powershot $G2$ (about $3\,frames/second$, $8\,Mpixel$) was located above the apparatus; a Sony $DCR-VX2000E$ ($15\,frames/second$, $4.5\,Mpixel$) was located in front of the channel; a Panasonic $NV-MX300EG$ ($25\,frames/second$, $1.8\,Mpixel$) filmed the motion laterally. A centesimal clock, caught by all the video-cameras, was used to synchronize the films by post-processing. The video-cameras allowed us to capture the position of the moving front and to observe qualitatively the nature of the motion. The dense granular flow keeps on during the entire evolution of

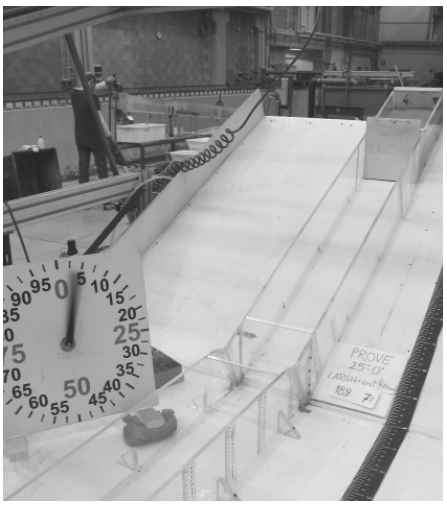

Fig. 5. The double slope chute with rectangular section (Toffolon (2006)).

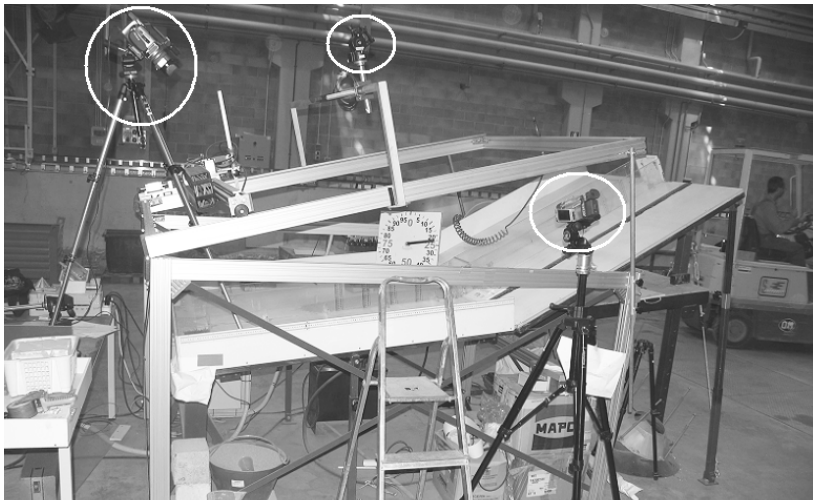

Fig. 6. The collocation of the three video-cameras used to shoot the evolution of the motion (Toffolon (2006)).

the motion, even after the abrupt slope reduction. For every experiment, pictures of the initial configuration and of the final deposit have been taken. In Table 1 and Table 2 are listed the laboratory experiments with constant width executed with the apparatus of Fig. 5 and Fig. 6.

The comparison between experimental results and numerical simulations

The experimental results have been used to compare the four versions of the numerical model. Hungr and Morgenstern (1984), through experiments executed with a annular shear cell, found that, in dynamic conditions, the friction angles reduce up to 4^o with respect to the static values. Deganutti and Scotton (1997) found a larger variability, from 3^o to 8^o, using a cone and plate rheometer and PVC granular material cylindrically shaped. So the numerical models have been tested with the static measured values of the internal and boundary friction angles and with dynamic values obtained reducing by 2^o and 4^o the static values. The results are shown in non-dimensional form in Fig. 7. Lengths are non-dimensionalized through the initial maximum depth H_s.

In Table 3 are reported the values of the stress coefficients for the various versions of the model in the case $\phi = 28^o$, $\delta_b = 22^o$, $\delta_{lat} = 18^o$.

For all the versions of the model, reducing the lateral friction angle a more thick final deposit is observed. The reduction of the bottom friction angle results in a more advanced front. The version $v1.3.3.1$ of the model gives the most elongated deposits. The reason is that the lateral pressure coefficient $k_{HH} = k_{\eta\eta}$

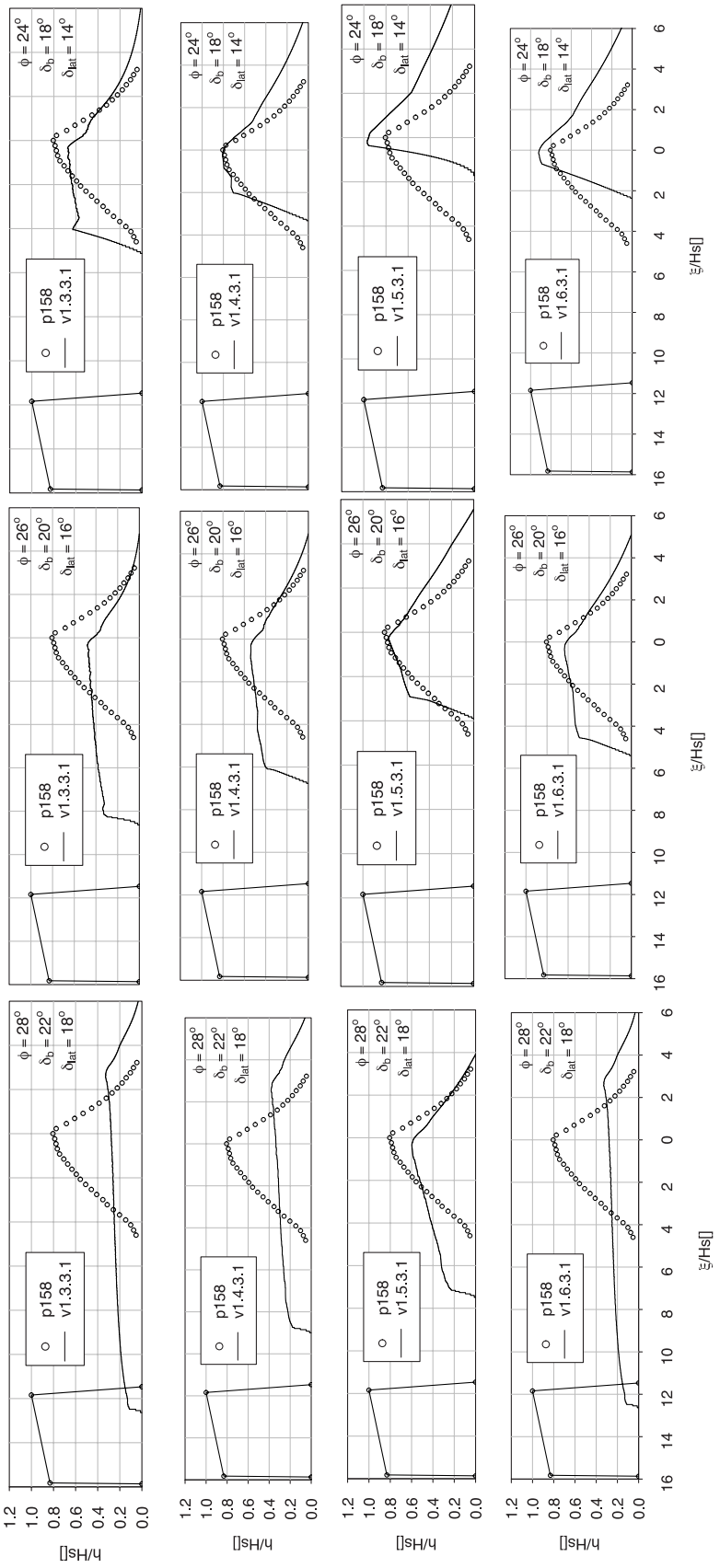

Fig. 7. The comparison of the initial and final configuration for experiment $p158$ and the numerical simulations obtained with the four different versions of the model and with three different sets of the internal, bottom and lateral friction angles. ξ and h are non-dimensionalized through $H_s = 0.087\,m$.

Table 1. Experiments executed in the chute with constant width equal to 10 *cm*.

width = 10 cm			
Exp. n.	**Upstream slope** [°]	**Downstream slope** [°]	**Initial volume** $[\mathbf{10^{-3}\ m^3}]$
158	25	0.1	3
159	25	0.1	3
160	25	0.1	7
161	25	0.1	7
162	30	0.1	3
163	30	0.1	3
164	30	0.1	6
165	30	0.1	6
166	25	7	3
167	25	7	3
168	25	7	7
169	25	7	7
170	30	7	3
171	30	7	3
172	30	7	6
173	30	7	6

Table 2. Experiments executed in the chute with constant width equal to 20 *cm*.

width = 20 cm			
Exp. n.	**Upstream slope** [°]	**Downstream slope** [°]	**Initial volume** $[\mathbf{10^{-3}\ m^3}]$
174	30	7	3
175	30	7	3
176	30	7	7
177b	30	7	7
178	25	7	7
179	25	7	7
180	25	7	3
181	25	7	3
182	30	0	3
183	30	0	3
184	30	0	7
185	30	0	7
186	25	0	3
187	25	0	3
188	25	0	7
189	25	0	7

is always greater than 1, being the ratio between the longitudinal pressure coefficient $k_{\Xi\Xi} = k_{\xi\xi}$ and the transversal pressure coefficient $k_{HH} = k_{\eta\eta}$ an active coefficient (see equation 8). Being the lateral friction tangential stress greater, the running depth results smaller. Conversely the most thick final deposit is obtained with version $v1.5.3.1$. In this case $k_{\eta\eta}$ is smaller, given by the ratio between $k_{\xi\xi}$ and a passive type coefficient (equation 9). The lateral friction tangential stress is consequently smaller. In version $v1.6.3.1$ the range of variation of $k_{\eta\eta}$ is reduced with respect to $v1.5.3.1$, imposing that $k_{\eta\eta} = k_{\xi\xi}$ when the mass is longitudinally lengthening (equation 10). In version $v1.4.3.1$ the lateral pressure is assumed hydrostatic ($k_{\eta\eta} = 1$), without any discrimination between active and passive conditions. The results of versions $v1.6.3.1$ and $v1.4.3.1$ are comprehended between the ones of versions $v1.3.3.1$ and $v1.5.3.1$.

The best fitting is given by version $v1.5.3.1$, with the static values of friction angles. This suggests that, in the analyzed cases with constant width, lateral pressures are much smaller than longitudinal pressures. Reducing the friction angles to the dynamic values, the results obtained with the other versions improve, but the front is too advanced and the deposit too long.

In Fig. 8, Fig. 9 and Fig. 10 are reported the comparison between the experimental data, relevant to

Table 3. Values of the stress coefficient for the four different versions of the model in thickening and elongating conditions.

	v1.3.3.1		**v1.4.3.1**		**v1.5.3.1**		**v1.6.3.1**	
	elongating	thickening	elongating	thickening	elongating	thickening	elongating	thickening
$\mathbf{k}_{\xi\xi}$	0.78	2.35	0.78	2.35	0.78	2.35	0.78	2.35
$\mathbf{k}_{\zeta\xi}$	0.4	0.4	0.4	0.4	0.4	0.4	0.4	0.4
$\mathbf{k}_{\eta\eta}$	1.28	3.84	1	1	0.31	0.93	0.78	0.93
$\mathbf{k}_{\eta\xi}$	0.42	1.25	0.32	0.32	0.1	0.3	0.25	0.3

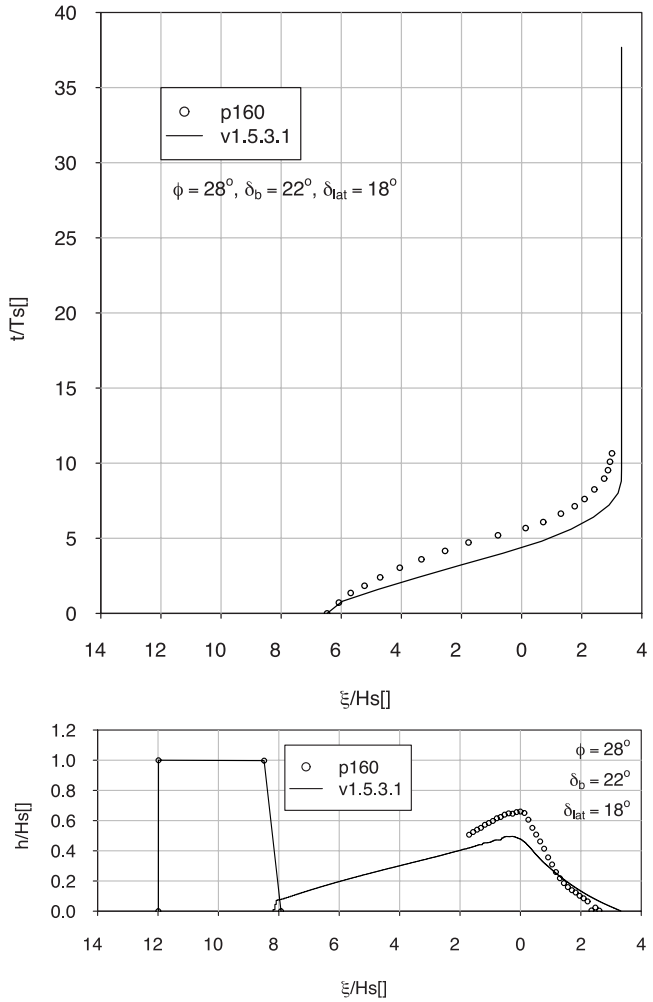

Fig. 8. Comparison between experimental data and numerical results obtained with version $v1.5.3.1$ of the model, $\phi = 28^o$, $\delta_b = 22^o$, $\delta_{lat} = 18^o$, for experiment $p160$. In the two images are represented the temporal evolution of the position of the front and the final deposit. ξ and h are non-dimensionalized through $H_s = 0.1\,m$; t through $T_s = 0.1\,s$.

experiments executed with different geometrical configurations of the chute (see Table 1 and Table 2), and the results of the simulations obtained with version $v1.5.3.1$, using the static values of the friction angles. The graphs report the temporal evolution of the position of the front and the final deposit. Spatial variables ξ and η are non-dimensionalized through H_s, the maximum initial depth of the deposit. Time t is non-dimensionalized through the time scale T_s. The fitting of the position and of the final shape of the front is quite accurate. Conversely, the final shape of the back is poorly fitted. Being the rear very elongated during the motion, it is difficult to recognize its end and so its temporal evolution has not been reported.

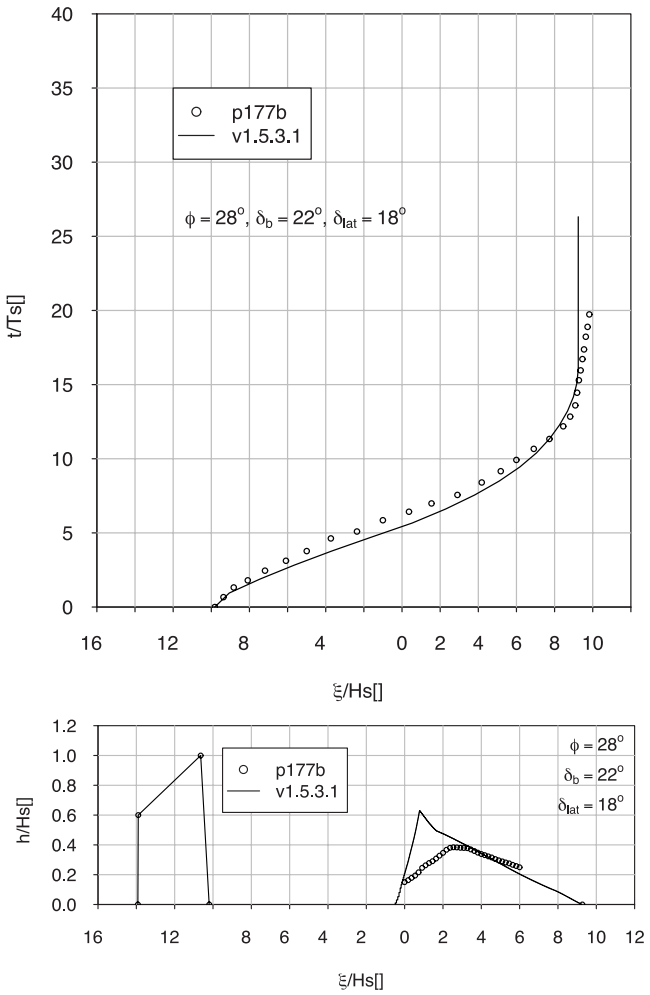

Fig. 9. Comparison between experimental data and numerical results obtained with version $v1.5.3.1$ of the model, $\phi = 28^o$, $\delta_b = 22^o$, $\delta_{lat} = 18^o$, for experiment $p177b$. In the two images are represented the temporal evolution of the position of the front and the final deposit. ξ and h are non-dimensionalized through $H_s = 0.11\,m$; t through $T_s = 0.11\,s$.

Conclusions

In this article a one dimensional model for the dynamic of confined granular avalanches, based on the theory of Savage and Hutter, has been introduced. A rheological model for the definition of the three dimensional stress tensor for granular materials in confined motion has not been developed yet. Four different hypotheses for the representation of the interaction of the moving mass with lateral boundaries have been discussed, showing the results of the corresponding versions of the model in the simulation of experimental cases, carried out at the Hydraulic Laboratory of the University of Trento, on a double slope chute with constant width. The extreme variability of the results indicates that a correct representation of the transversal pressure is fundamental, but the simulations do not give certain suggestions for the best rheological choice. In the version of the model which gives the best fittings of the experimental data, the values of the transversal pressure coefficient are small compared to the values of the longitudinal pressure coefficient, and vary whether the mass is elongating or thickening in the longitudinal direction. Nevertheless unresolved aspects still persist. The best results are obtained with the static, and not the dynamic values of friction angles. The law of distribution of the stress tensor along the transversal direction η affects the ratio, in the averaged equation 13, between the resistance to the motion at the bottom and at the banks. The hypothesis of a linear law distribution can fail, specially when the width is much greater than the moving depth, and has to be further tested. Applying the model to variable width cases, the criterion for the discrimination between active and passive transversal conditions has to be extended. Other effects can take place, like the separation of the flux from the sides. It is conceivable that the transition between active and passive state is gradual and yield conditions can occur on the plane ΞH only in extreme cases. So the transversal pressure depends on the deformation history of

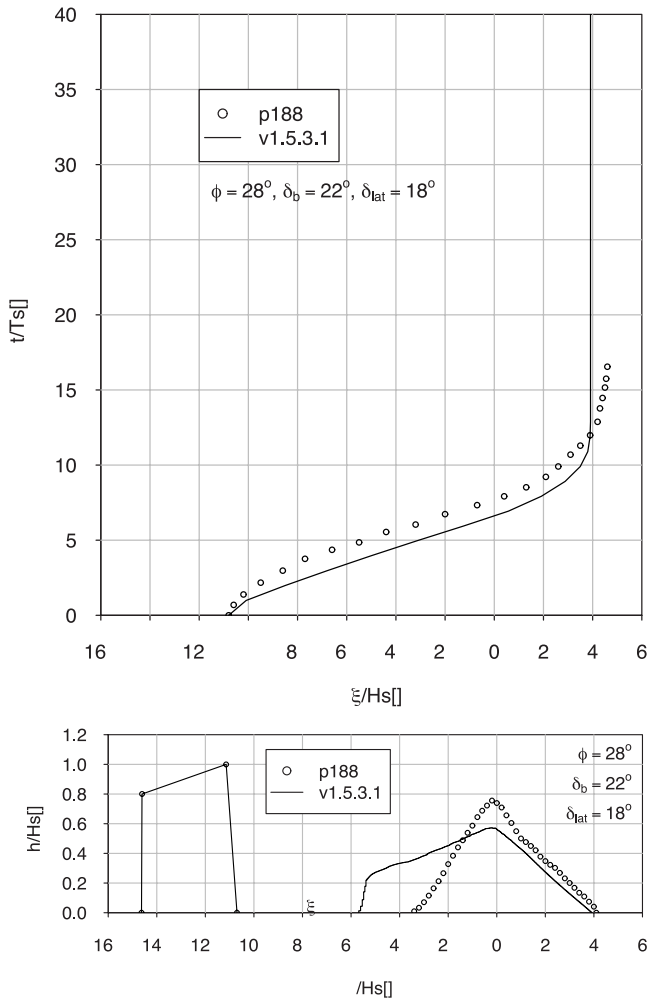

Fig. 10. Comparison between experimental data and numerical results obtained with version $v1.5.3.1$ of the model, $\phi = 28^o$, $\delta_b = 22^o$, $\delta_{lat} = 18^o$, for experiment $p188$. In the two images are represented the temporal evolution of the position of the front and the final deposit. ξ and h are non-dimensionalized through $H_s = 0.15\,m$; t through $T_s = 0.12\,s$.

the moving mass and its definition is not univocal. A new laboratory campaign is in project to measure the normal pressure and the tangential stress at lateral wall, in order to study a physically based theory to define the three dimensional stress tensor.

References

Barberi, M. and Scotton, P. (2004) Avalanche risk analysis and management in Mite Valley (Val di Sole, Italy). *INTERPRAEVENT 2004*, Band 2, p.VI/1–VI/12.

Deganutti, A., and Scotton, P. (1997) Yield stress of granular material. *Debris-Flow Hazard Mitigation: Mechanism, Prediction and Assessment*, ed. Cheng-Lung Chen, ASCE, 270–278.

De Toni, S., Scotton, P. and Bertolazzi, E. (2004) Two dimensional mathematical and numerical model for the dynamics of granular avalanches. *INTERPRAEVENT 2004*, Band 2, p.VI/103–VI/114.

De Toni, S. (2005) *A two dimensional model for the dynamics of granular avalanches.* Doctoral Thesis in Environmental Engineering, University of Trento, p.148.

De Toni, S. and Scotton, P. (2005) Two-dimensional mathematical and numerical model for the dynamics of granular avalanches. *Cold Region Science and Technology* **43**, 36–48.

Hungr O. and Morgenstern N. (1984) Experiments on the flow behaviour of granular materials at high velocity in an open channel. *Geotechnique* **34**, 405–413.

Hutter, K., Siegel, M., Savage, S. B., Nohguchi, Y. (1993) Two–dimensional spreading of a granular avalanche down an inclined plane Part I. theory. *Acta Mechanica* **100**, Issue 1–2, 37–68.

Pudasaini, S.P. and Hutter, K. (2003) Rapid shear flows of dry granular masses down curved and twisted channels. *Journal of Fluid Mechanics* **495**, 193–208.

Pudasaini, S.P., Wang, Y. and Hutter, K. (2004) Dynamics of avalanches along general mountain slopes. *Annals of Glaciology* **38**, 357–362.

Pudasaini, S.P., Wang, Y. and Hutter, K. (2005) Rapid motions of free-surface avalanches down curved and twisted channels and their numerical simulation. *Philosophical Transaction of the Royal Society A* **363**, 1551–1571.

Savage, S.B. and Hutter, K. (1989) Motion of granular material down a rough incline. *Journal of Fluid Mechanics* **199**, 177–215.

Savage, S. B. and Hutter, K. (1991) The dynamics of avalanches of granular materials from initiation to runout. Part i. *Acta Mechanica* **86**, 201–223.

Scotton, P. (1999) *Studio dei Fenomeni Valanghivi della Val dei Spini (Comune di Pejo, Trento). Relazione Finale.* Technical Report, Contract between University of Trento and Regional Council of Trento n. 3579/97-C33-N.

Toffolon, C. (2006) *Calibrazione sperimentale di un modello monodimensionale a larghezza variabile per valanghe di neve densa.* Degree Thesis in Environmental Engineering, University of Trento.